H_∞ Optimization of Luenberger State Observers and Its Application to Fault Detection Filter Design

Soichi Ibaraki
Department of Precision Engineering,
Kyoto University, Kyoto 606-8501, Japan
ibaraki@prec.kyoto-u.ac.jp

Shashikanth Suryanarayanan[1] and Masayoshi Tomizuka[2]
Department of Mechanical Engineering,
University of California at Berkeley, Berkeley, CA 94720-1740
[1]shashi@mechatro2.me.berkeley.edu [2]tomizuka@me.berkeley.edu

Abstract

This paper considers H_∞ optimization of Luenberger state observers. The conventional formulation of H_∞-optimal state observers does not allow the augmentation of dynamic performance weightings in the optimization objective, since it makes the problem a nonconvex optimization problem. We propose an algorithm to locally solve an H_∞ optimization problem of Luenberger state observers by transforming the problem into an H_∞ optimization problem of a static output feedback controller. The proposed approach offers an intuitive and efficient way to explicitly design the estimation error dynamics of the observer in the frequency domain. As an application example, the proposed approach is applied to the tuning of fault detection filters for lateral control of automated passenger vehicles. Numerical simulations are conducted to show the effectiveness of the proposed tuning method.

1 Introduction

Optimal state estimation (or filtering) problems have been studied for decades in parallel with optimal control problems. In particular, this paper considers the H_∞-optimal state observer and its application to fault detection filter design.

The H_∞-optimal filtering problem was first addressed in the late-1980s by Elsayed and Grimble [1] based on polynomial techniques. In 1991, Nagpal and Khargonekar [2] presented the ARE-based formulation of H_∞-optimal state observers. It was shown that the H_∞ optimization problem of Luenberger state observers for an LTI (linear time invariant) system could be, analogous to the H_2 optimization case, reparameterized as a problem to solve a set of algebraic Ricatti equations (AREs). However, compared to the popularity that the celebrated Kalman filter (H_2-optimal state observer) has enjoyed, there has not been as many practical applications of H_∞-optimal state observers reported in the literature.

This paper proposes the application of the frequency-domain loop shaping approach to the design of Luenberger state observers. It offers an intuitive and efficient method to explicitly design the estimation error dynamics in the frequency domain. For this purpose, the augmentation of dynamic performance weightings in the optimization objective is crucial. The conventional formulation of H_∞ state observers does not, however, allow the augmentation of dynamic weightings, since it makes the problem a nonconvex optimization problem. This paper presents an extension of the conventional H_∞ optimization algorithm of Luenberger state observers to more general problems with dynamics weightings.

It should be noted that nonconvex H_∞ optimization problems of state observers have attracted more attention in recent years, mainly from the interest in the design of robust filters (e.g. [3, 4, 5]). Although the approach proposed in this paper does not explicitly deal with the robustness issue, it offers a simple and effective way to incorporate the designer's expertise and understanding of the physical system and design objectives into the observer design.

The remainder of this paper is organized as follows. Section 2 proposes an algorithm to solve an H_∞ optimization problem of Luenberger state observers with dynamic weightings. In Section 3, the proposed approach is applied to the design of fault detection filters for lateral control of automated passenger vehicles.

2 H_∞ Optimization of Luenberger State Observers with Dynamic Weightings

The H_∞ optimization problem of Luenberger state observers is formulated as follows. Consider an LTI system of the following state-space representation:

$$P(s): \quad \begin{aligned} \dot{x}(t) &= Ax(t) + Bu(t) + B_w w(t) \\ y(t) &= Cx(t) + D_w w(t) \end{aligned} \tag{1}$$

where $x(t) \in \mathbb{R}^n$ is the state vector, $u(t) \in \mathbb{R}^{m_1}$ is the control input, $y(t) \in \mathbb{R}^{p_1}$ is the measured output, and $w(t) \in \mathbb{R}^{m_2}$ denotes the noise or external disturbances.

The Luenberger state observer has the following structure:

$$\hat{P}(s): \quad \dot{\hat{x}}(t) = A\hat{x}(t) + Bu(t) + L(y - C\hat{x}(t)) \tag{2}$$

where $L \in \mathbb{R}^{n \times p_1}$ is the observer gain matrix and $\hat{x}(t) \in \mathbb{R}^n$ is the estimated state vector. Notice that

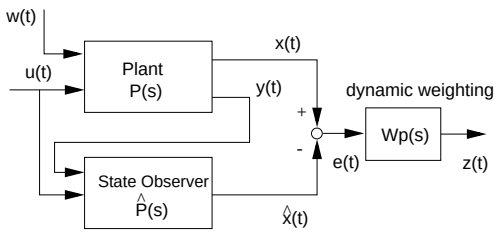

Figure 1: Block diagram of state estimation error dynamics

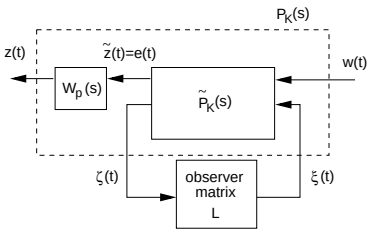

Figure 2: Extraction of the observer matrix, L

the system matrices of the observer coincide with those of the plant model.

The objective is to optimize the observer matrix, L, such that the H_∞ norm of the transfer function matrix from the external disturbance, $w(t)$, to the weighted state estimation error, $z(t)$, is minimized (denote this transfer function matrix by $T_{w\to z}(s)$). $z(t)$ is defined in the s-domain as follows:

$$z(s) = W_p(s)(x(s) - \hat{x}(s)) \tag{3}$$

where $W_p(s)$ is a $p_2 \times n$ weighting transfer function matrix. The block diagram of $T_{w\to z}(s)$ is shown in Figure 1.

When the weighting matrix, $W_p(s)$, is a static matrix, i.e. $W_p(s) = W_p \in \mathbb{R}^{p_2\times n}$, the H_∞ problem of the observer matrix, L, can be reparameterized as an LMI (linear matrix inequality) problem [6], or equivalently, a problem to solve a set of AREs shown by Nagpal and Khargonekar [2].

However, when a dynamic weighting matrix, $W_p(s)$, is augmented, it can be easily seen that this problem cannot be rewritten as an LMI problem by using the variable transformation. When dynamic weights are augmented, the state observer, $\hat{P}(s)$, is no longer a full state estimator, since the state variables of dynamic weights are not estimated (they do not exist in the physical system). Notice that the analogous observation applies to the H_∞ synthesis problem of state feedback controllers.

We apply the H_∞ optimization algorithm for fixed-structure controllers presented by Ibaraki and Tomizuka [7] to locally solve this problem. The algorithm proposed in [7] first transforms an H_∞ optimization problem of fixed-structure controllers into an synthesis problem of a static output feedback controller by "extracting" tunable controller parameters using linear fractional transformations (LFTs). This approach can be straightforwardly applied to the H_∞ optimization problem of Luenberger state observers.

To illustrate the transformation, first consider the transfer function from $w(t)$ to the state estimation error vector, $e(t) := x(t) - \hat{x}(t)$, without a dynamic weighting matrix, $W_p(s)$. By combining the plant dynamics (1) and the observer dynamics (2), the state estimation error dynamics is given as follows:

$$\dot{e}(t) = (A - LC)e(t) + B_w w(t)\,. \tag{4}$$

Then, construct the extended plant model $\tilde{P}_K(s)$ as follows (see Figure 2):

$$\begin{aligned} \dot{e}(t) &= Ae(t) + B_w w(t) - \xi(t) \\ \tilde{z}(t) &= e(t) \\ \zeta(t) &= Ce(t)\,. \end{aligned} \tag{5}$$

It is easy to see that $F_L(\tilde{P}_K(s), L)$ is equal to the state estimation error dynamics, $T_{w\to e}(s)$, where $F_L(\tilde{P}_K(s), L)$ denotes the closed-loop transfer function from $w(t)$ to $\tilde{z}(t)$ in Figure 2. When a dynamic weighting matrix $W_p(s)$ is augmented, let $P_K(s)$ be the serial combination of $\tilde{P}_K(s)$ and $W_P(s)$ as shown in Figure 2. Then, $F_L(P_K(s), L)$ becomes equal to the transfer function from $w(t)$ to $z(t)$.

Notice that the observer matrix, L, is a constant $n \times p_1$ full block matrix whose entries are all independently tunable. *Therefore, the* H_∞ *optimization problem of the observer matrix,* L*, can be seen as an* H_∞ *synthesis problem of a static output feedback controller for the extended plant model,* $\mathrm{P_K(s)}$. Although it is generally hard to globally solve an H_∞ synthesis problem of a static output feedback controller, the cone complementarity linearization algorithm proposed by El Ghaoui et al. [8] can be straightforwardly applied to locally solve this problem. Although it is a local search algorithm and thus is not always guaranteed to find the global minimum, in many practical applications it performs excellent, as reported in [8] with extensive numerical examples.

3 Application Example

3.1 Fault Management in Lateral Control of Automated Vehicles

As an application example in which the frequency-domain estimation error performance of a Luenberger state observer is particularly important, the proposed approach is applied to the design of fault detection filters for lateral control of automated passenger vehicles.

The design of reliable, fault-tolerant control systems requires that system failures be detected and identified such that the system feedback is not excessively corrupted. Fault detection and isolation (FDI) problems in dynamic systems have been an active research area in recent years. In particular, this paper focuses on the state estimator design in model-based fault detection

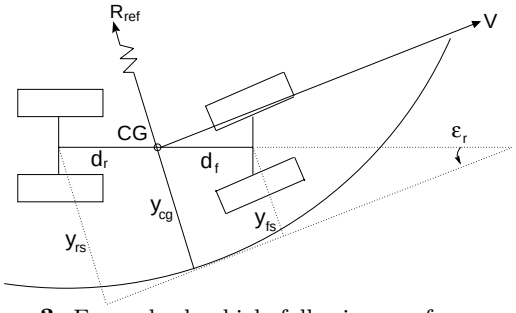

Figure 3: Four-wheel vehicle following a reference path

schemes (e.g. [9]).

Rajamani et al. [10] developed a complete fault diagnostic system for automated passenger vehicles, which detects and identifies all possible faults in twelve sensors and three actuators (e.g. wheel speed sensor, throttle angle sensor, magnetometers, brake actuator) used in lateral and longitudinal control systems of the vehicle. A bank of state observers, each of which is based on different combination of sensor outputs, generates residuals to detect and isolate each possible fault. This section focuses only on a fault detection scheme for two sets of magnetometers to measure lateral displacements of the vehicle. It can be seen as a subsystem of a complete fault diagnostic system. The same approach can be applied to the tuning of any fault detection filters.

3.2 Model Description

The design of fault detection filters is based on the simplified lateral motion model of a passenger vehicle presented by Hingwe [11, Chapter 3]. Figure 3 shows a front-wheel steered vehicle model on a curve of radius R_{ref}. Magnets buried along the highway center lane are utilized as a reference for the lane following operation. Magnetometers mounted on the front and rear bumpers of the vehicle are used to measure the lateral deviation of the vehicle from the road center line.

The "bicycle model" presented in [11] neglects the roll and pitch motions in the vehicle and assumes that the relative yaw angle is maintained small. Under these assumptions, the lateral motion of the vehicle can be represented by the following linearized model:

$$\begin{aligned} \dot{x} &= Ax + B_1\delta + B_2\dot{\epsilon}_d \\ \begin{bmatrix} y_{fs} \\ y_{rs} \end{bmatrix} &= \begin{bmatrix} 1 & 0 & d_f & 0 \\ 1 & 0 & -d_r & 0 \end{bmatrix} x =: Cx \end{aligned} \quad (6)$$

where $x = [\ y_{cg} \quad \dot{y}_{cg} \quad \epsilon_r \quad \dot{\epsilon}_r\ ]^T$ is the state variable vector: y_{cg} is the lateral displacement of the vehicle's center of gravity (CG) relative to the road centerline, and ϵ_r is the yaw angle of the vehicle relative to the road centerline (See Figure 3). δ is the steering angle and it is the control input. $\dot{\epsilon}_d$ is the yaw rate of the road frame and is regarded as a disturbance. See [11] for detailed descriptions of the system matrices, $A \in \mathbb{R}^{4\times4}$ and $B_1,\ B_2 \in \mathbb{R}^{4\times1}$. y_{fs} and y_{rs} are lateral errors

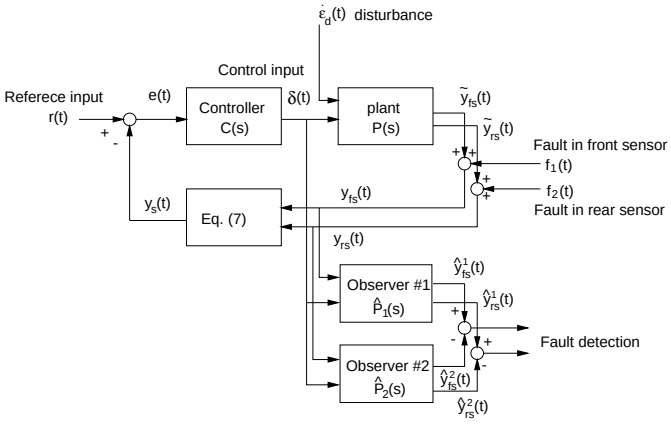

Figure 4: Block diagram of fault detection scheme based on dedicated observers

measured by magnetometers at the front bumper and the rear bumper, respectively.

A SISO (single-input single-output) linear controller was implemented for lateral control of the vehicle in lane-following maneuvers. The input to the controller is defined as follows:

$$y_s = \frac{d_2 + d_s}{d_1 + d_2} y_{fs} + \frac{d_1 - d_s}{d_1 + d_2} y_{rs} \quad (7)$$

where d_s is constant and can be arbitrarily specified. The controller, $C(s)$, is essentially given as the combination of a second-order linear lead-lag filter and a notch filter to account for roll-yaw coupling. It was successfully implemented on a test vehicle and its control performance was verified in simulation and experimentation. The closed-loop configuration of the entire lateral control system is depicted in Figure 4.

3.3 Fault Detection Scheme

Figure 4 includes the fault detection architecture for magnetometers. The dedicated state observer #1, $\hat{P}_1(s)$, estimates y_{fs} and y_{rs} by using measured y_{fs} and the steering angle, δ. Denote its estimates by $\hat{y}^1_{fs}$ and $\hat{y}^1_{rs}$. The dedicated state observer #2, $\hat{P}_2(s)$, estimates the same two variables based on measured y_{rs} and δ. Denote its estimates by $\hat{y}^2_{fs}$ and $\hat{y}^2_{rs}$.

The magnetometer fault considered here appears as an offset on sensor measurements, y_{fs} and y_{rs}. Furthermore, faults are assumed not to occur in both magnetometers simultaneously. Two dedicated state observers, $\hat{P}_1(s)$ and $\hat{P}_2(s)$, are designed such that the differences of their estimates, $\hat{y}^1_{fs} - \hat{y}^2_{fs}$ and $\hat{y}^1_{rs} - \hat{y}^2_{rs}$, are kept smaller than the prescribed constant levels during non-faulty operations. Suppose that, for example, a fault occurred in the front sensor. Then, the dedicated observer #1 can no longer estimate the correct lateral errors, since it is based on faulty sensor measurement, while the observer #2 is not affected by this fault. Therefore, by monitoring the difference of each observer's estimates, one can detect the fault. This is

a basic idea of the dedicated observer based fault detection scheme.

A critical issue in the design of such dedicated observers is the robustness against external disturbances and model uncertainties. In particular, the most significant disturbance to the lateral dynamics of the vehicle is the centering force at curved roads, which acts mostly as a static disturbance. Since a magnetometer fault also appears as a static offset, steady-state estimation errors of dedicated observers must be small to distinguish faults from static disturbances.

Suryanarayanan and Tomizuka [12] proposed a fault tolerant controller for lateral control of automated passenger vehicles, which guarantees the stability of the closed-loop system even when one of magnetometers is lost. It consists of two dedicated state observers and the state feedback based on their estimates. The architecture of dedicated observers is exactly the same as the one shown in Figure 4. Therefore, the fault detection scheme presented in this section can be implemented without adding any redundancy on this fault tolerant control architecture.

3.4 Design Procedure of Dedicated Observers

Design Objectives: The dedicated state observers, $\hat{P}_1(s)$ and $\hat{P}_2(s)$, have the following Luenberger-type state observer structures:

$$\begin{aligned}
\hat{P}_1(s): \quad \dot{\hat{x}}_1 &= A\hat{x}_1 + B_1\delta + L_1(y_{fs} - \hat{y}^1_{fs}) \\
\begin{bmatrix} \hat{y}^1_{fs} \\ \hat{y}^1_{rs} \end{bmatrix} &= C\hat{x}_1\,, \\
\hat{P}_2(s): \quad \dot{\hat{x}}_2 &= A\hat{x}_2 + B_1\delta + L_2(y_{rs} - \hat{y}^2_{rs}) \\
\begin{bmatrix} \hat{y}^2_{fs} \\ \hat{y}^2_{rs} \end{bmatrix} &= C\hat{x}_2\,, \qquad (8)
\end{aligned}$$

The observer system matrices, (A, B_1, C), coincide with those of the plant model given in Eq. (6).

First, the observer matrices, L_1 and L_2, were obtained by using the Kalman filter design, as demonstrated in [12]. Denote these Kalman filters as $\hat{P}_1^{old}(s)$ and $\hat{P}_2^{old}(s)$. When $\hat{P}_1^{old}(s)$ and $\hat{P}_2^{old}(s)$ are used, frequency responses of estimation error dynamics from the external disturbance, $\dot{\epsilon}_d$, to the estimation error, $e_{fs} := y_{fs} - \hat{y}_{fs}$ and $e_{rs} := y_{rs} - \hat{y}_{rs}$, are given as shown in Figure 5 (dashed lines). Denote these transfer functions by $T_{\dot{\epsilon}_d \to e_{fs}}(s)$ and $T_{\dot{\epsilon}_d \to e_{rs}}(s)$, respectively.

The figure implies that $\hat{P}_1^{old}(s)$ and $\hat{P}_2^{old}(s)$ are not effective for the fault detection purpose by the following reasons: 1) the steady state gains of error dynamics are not sufficiently small, especially that of $\hat{P}_2^{old}(s)$ in the $T_{\dot{\epsilon}_d \to e_{fs}}(s)$ dynamics (the upper-left figure), and 2) the differences of steady state errors of $\hat{P}_1^{old}(s)$ and $\hat{P}_2^{old}(s)$ are not sufficiently small, especially that in the $T_{\dot{\epsilon}_d \to e_{fs}}(s)$ dynamics (the upper-left figure). Since the fault detection scheme is based on the differences of two observers' estimates, they must be small during non-faulty operation.

Time domain simulations, which will be presented in Section 3.5, also show that $\hat{P}_1^{old}(s)$ and $\hat{P}_2^{old}(s)$ are not effective for the fault detection purpose. The objective of this section is to re-tune the observer matrices, L_1 and L_2, such that both observers show desirable estimation error dynamics for more accurate fault detection.

Design of $\hat{P}_2(s)$: It is easy to see that the problem to optimize L_1 and L_2 at the same time cannot be transformed into a static output feedback synthesis problem as shown in Section 2. Therefore, L_1 and L_2 are optimized in an alternating manner to obtain a locally optimal solution, similarly as shown in [6, Section 3.6] for fixed-structure controller optimization cases.

First, consider the tuning problem of L_2, with L_1 fixed to the Kalman filter gain obtained above. The tuning objective is to reduce the gain of estimation error dynamics especially at lower frequencies, without sacrificing the estimation stability. It can be interpreted as an H_∞ optimization problem as follows:

$$\min_{L_2} \quad \left\| \begin{array}{c} W_{p1}(s) T^2_{\dot{\epsilon}_d \to e_{fs}}(s) \\ W_{p2}(s) T^2_{\dot{\epsilon}_d \to e_{rs}}(s) \end{array} \right\|_\infty \qquad (9)$$

where $T^2_{\dot{\epsilon}_d \to e_{fs}}(s)$ and $T^2_{\dot{\epsilon}_d \to e_{rs}}(s)$ denote the estimation error dynamics of the dedicated observer #2, $\hat{P}_2(s)$. $W_{p1}(s)$ and $W_{p2}(s)$ are dynamic performance weightings, which specify the desired shapes of $|T^2_{\dot{\epsilon}_d \to e_{fs}}(j\omega)|$ and $|T^2_{\dot{\epsilon}_d \to e_{rs}}(j\omega)|$, respectively. $W_{p1}(s)$ and $W_{p2}(s)$ are designed based on actual frequency responses of $T^2_{\dot{\epsilon}_d \to e_{fs}}(s)$ and $T^2_{\dot{\epsilon}_d \to e_{rs}}(s)$ when the Kalman filter, $\hat{P}_2^{old}(s)$, is used, such that the solution of the problem (9) achieves better performance than the Kalman filter. The analogous "loop-shaping" technique to design performance filters in the optimization setting is widely used in the H_∞ controller design (see [7]). "Wp1" and "Wp2" in Figure 6 represent the inverse frequency responses of $W_{p1}(s)$ and $W_{p2}(s)$, respectively.

All computations to solve the problem (9) have been carried out on *MATLAB* by using *LMI Control Toolbox* [13]. The (sub-)optimal solution, denoted by $\hat{P}_2^{new}(s)$, achieves the H_∞ norm (9) of 1.425, while $\hat{P}_2^{old}(s)$ gives 15.91. Figure 6 compares the frequency responses of estimation error dynamics of $\hat{P}_2^{old}(s)$ and $\hat{P}_2^{new}(s)$. The gain reduction at lower frequencies can be clearly observed in both error dynamics.

Design of $\hat{P}_1(s)$: Then, consider the tuning problem of L_1, with L_2 fixed to the value obtained above. Since the fault detection scheme is based on estimation gaps of two observers, they must be small during non-faulty operations. Considering this requirement, the optimization objective for L_1 is given as follows:

$$\min_{L_1} \quad \left\| \begin{array}{c} W_{p1}(s)(T^1_{\dot{\epsilon}_d \to e_{fs}}(s) - T^2_{\dot{\epsilon}_d \to e_{fs}}(s)) \\ W_{p2}(s)(T^1_{\dot{\epsilon}_d \to e_{rs}}(s) - T^2_{\dot{\epsilon}_d \to e_{rs}}(s)) \end{array} \right\|_\infty \qquad (10)$$

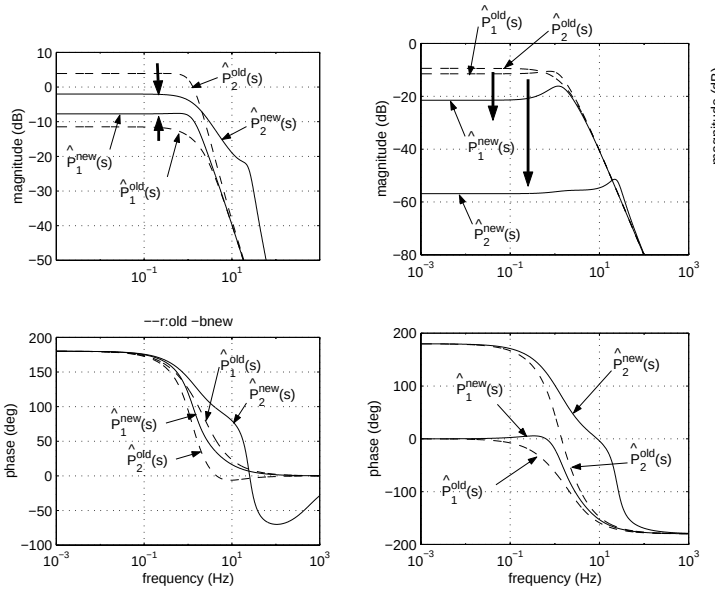

(a) Estimation error dynamics of y_{fs}, $|T_{\dot{\epsilon}_d \to e_{fs}}(j\omega)|$ (b) Estimation error dynamics of y_{rs}, $|T_{\dot{\epsilon}_d \to e_{rs}}(j\omega)|$

Figure 5: Comparison of estimation error dynamics of the Kalman filters, $P_1^{old}(s)$ and $P_2^{old}(s)$, and the re-tuned settings, $P_1^{new}(s)$ and $P_2^{new}(s)$

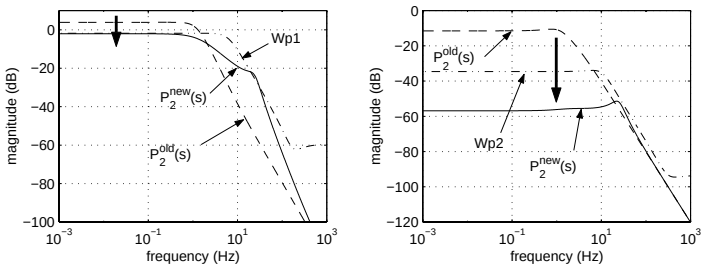

(a) Estimation error dynamics of y_{fs}, $|T_{\dot{\epsilon}_d \to e_{fs}}(j\omega)|$ (b) Estimation error dynamics of y_{rs}, $|T_{\dot{\epsilon}_d \to e_{rs}}(j\omega)|$

Figure 6: Comparison of estimation error dynamics of the Kalman filter, $P_2^{old}(s)$, and the re-tuned setting, $P_2^{new}(s)$

where $T^1_{\dot{\epsilon}_d \to e_{fs}}(s)$ and $T^1_{\dot{\epsilon}_d \to e_{rs}}(s)$ denote the estimation error dynamics of the dedicated observer #1, $\hat{P}_1(s)$. In this problem, the performance weightings, $W_{p1}(s)$ and $W_{p2}(s)$, are set to $W_{p1}(s) = W_{p2}(s) = 1$.

Since $\hat{P}_2(s)$ is fixed, the problem (10) can be also transformed to an H_∞ optimization problem of a static output feedback gain matrix. The (sub-)optimal solution, denoted by $\hat{P}_1^{new}(s)$, achieves the H_∞ norm (10) of 0.400, while $\hat{P}_1^{old}(s)$ gives 0.626. Figure 5 compares estimation error dynamics of the Kalman filters, $\hat{P}_1^{old}(s)$ and $\hat{P}_2^{old}(s)$ (dashed lines), and the re-tuned observers, $\hat{P}_1^{new}(s)$ and $\hat{P}_2^{new}(s)$ (solid lines). In Figure 5 (a), it can be observed that the steady state error of $\hat{P}_2(s)$ was reduced by the tuning, while that of $\hat{P}_1(s)$ was slightly increased to reduce the gap between two observers. Figure 5 (b) shows that the steady state errors of two observers were both significantly reduced and, therefore, the difference of steady state errors was also reduced.

Since no significant improvement was achieved by further iterations, the design procedure was terminated at this point.

3.5 Simulation Results

Time domain simulations were conducted to show the effectiveness of the proposed tuning method of dedicated state observes. Figure 7 shows simulated estimation responses of the Kalman filters, $\hat{P}_1^{old}(s)$ and $\hat{P}_2^{old}(s)$. A fault occurs in the front magnetometer at the distance 220 m, when the vehicle is on a curved road of radius 800 m. The fault results in an offset of 0.05 m in the y_{fs} measurement. The plant model is assumed to be in the nominal condition: M (sprung mass of the vehicle) = 1740 kg, μ (road adhesion coefficient) = 0.85, and v (longitudinal velocity of the vehicle) = 15 m/s (=54 km/hr).

The estimation gap of two observers, $\hat{y}^1_{fs} - \hat{y}^2_{fs}$ and $\hat{y}^1_{rs} - \hat{y}^2_{rs}$, are shown in Figure 8. It can be observed that the steady-state amplitude of $\hat{y}^1_{fs} - \hat{y}^2_{fs}$ does not differ much before and after the fault occurred. Therefore, the fault cannot be detected by monitoring $\hat{y}^1_{fs} - \hat{y}^2_{fs}$. This is because the steady state estimation error of each observer is too large due to static disturbances even under non-faulty operations.

Then, the fault detection performance of the re-tuned dedicated observers, $\hat{P}_1^{new}(s)$ and $\hat{P}_2^{new}(s)$, was evaluated by using the same simulation scenario. Figure 9 shows the estimation gap profiles, $\hat{y}^1_{fs} - \hat{y}^2_{fs}$ and $\hat{y}^1_{rs} - \hat{y}^2_{rs}$, when $\hat{P}_1^{new}(s)$ and $\hat{P}_2^{new}(s)$ are used. The steady state errors between two observers became smaller during non-faulty operations, and thus the fault can be easily detected by setting the threshold values at $0.02 \sim 0.04\,m$ for both of $|\hat{y}^1_{fs} - \hat{y}^2_{fs}|$ and $|\hat{y}^1_{rs} - \hat{y}^2_{rs}|$. It was also verified by simulation that the designed observers can detect this fault even when measurement noise is added to the simulation model.

Finally, it should be noted that the present fault detection scheme is by nature robust against model uncertainties to some extent, although the robustness issue was not explicitly considered in the design of dedicated observers. Figure 10 shows the simulation results in two perturbed conditions ("p1": $M = 2,610\,kg$, $\mu = 1.0$, $v = 20\,m/s$) and ("p2": $M = 870\,kg$, $\mu = 0.5$, $v = 10\,m/s$). $\hat{P}_1^{new}(s)$ and $\hat{P}_2^{new}(s)$ can produce similar residuals at steady state even in perturbed conditions.

4 Conclusion

The conventional formulation of H_∞-optimal state observers does not allow the augmentation of dynamic performance weightings in the optimization objective, since it makes the problem a nonconvex optimization problem. This paper proposed an algorithm to locally

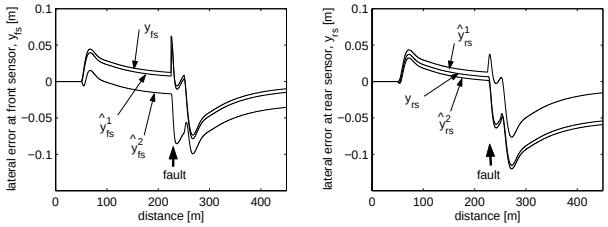

Figure 7: Measured and estimated lateral errors at the locations of the front sensor, y_{fs} (left), and the rear sensor, y_{rs} (right), when the Kalman filters, $\hat{P}_1^{old}(s)$ and $\hat{P}_2^{old}(s)$, are used (y_{fs} and y_{rs}: measured lateral errors, $\hat{y}_{fs}^1$ and $\hat{y}_{rs}^1$: estimation by $\hat{P}_1^{old}(s)$, $\hat{y}_{fs}^2$ and $\hat{y}_{rs}^2$: estimation by $\hat{P}_2^{old}(s)$)

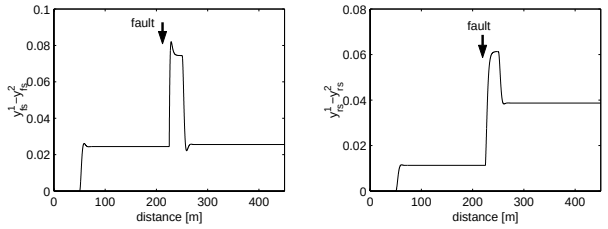

Figure 8: The estimation gap profiles, $\hat{y}_{fs}^1 - \hat{y}_{fs}^2$ (left) and $\hat{y}_{rs}^1 - \hat{y}_{rs}^2$ (right), corresponding to Figure 7

solve this problem by transforming the problem into an H_∞ optimization problem of a static output feedback gain matrix. Based on the proposed algorithm, this paper presented an intuitive and efficient way to explicitly design the estimation error dynamics of the observer in the frequency domain.

As an application example, the proposed approach was applied to the design of fault detection filters for lateral control of automated passenger vehicles. For accurate fault detection in vehicle control systems, the robustness of the dedicated observers against external disturbances of low frequencies is particularly important. The proposed approach was applied to re-tune the observer gain matrices of two dedicated observes. Simulation results showed the effectiveness of the proposed re-tuning method.

Acknowledgements

This work was in part supported by the California Department of Transportation under PATH MOU373.

References

[1] A. Elsayed and M. J. Grimble, "A new approach to the H_∞ design of optimal digital linear filters," *IMA J. of Mathematical Control and Information*, Vol. 6, No. 2, pp.233–251, 1989.

[2] K. M. Nagpal and P. P. Khargonekar, "Filtering and Smoothing in an H_∞ setting," *IEEE Trans. on Automatic Control*, Vol. 36, No. 2, pp. 152–166, 1992.

[3] L. Xie, C. E. de Souza, and M. Fu, "H_∞ estimation for discrete-time linear uncertain systems," *Int. J. of Robust Nonlinear Control*, Vol. 42, No. 10, pp. 111–123, 1991.

[4] H. D. Tuan, P. Apkarian, and T. Q. Nguyen, "Robust and reduced-order filtering: new characterizations and methods," *Proc. of the ACC*, Chicago, IL, pp. 1327–1331, June 2000.

[5] T. Song and E. G. Collins, Jr., "Robust H_2 estimation with application to robust fault detection," *Proc. of the ACC*, Chicago, IL, pp. 1200–1204, June 2000.

[6] S. Ibaraki, *Nonconvex Optimization Problems in H_∞ Optimization and Their Applications*, Ph.D. Thesis, Univ. of California at Berkeley, 2000.

[7] S. Ibaraki and M. Tomizuka, "H_∞ optimization of fixed structure controllers," *Proc. of the 2000 IMECE*, Orlando, FL, Nov. 2000.

[8] L. El Ghaoui, F. Oustry, and M. AitRami, "A cone complementarity linearization algorithm for static output-feedback and related problem," *IEEE Trans. on Automatic Control*, Vol. 42, No. 8, pp. 1171-1176, 1997.

[9] P. M. Frank, "Fault diagnosis in dynamic systems using analytical and knowledge-based redundancy — A survey and some new results," *Automatica*, Vo. 26, No. 3, pp. 459–474, 1990.

[10] R. Rajamani, A. Howell, C. Chen, J. K. Hedrick, and M. Tomizuka, "A complete fault diagnostic system for automated vehicles," *Proc. of the 14th IFAC World Congress*, Beijing, P. R. China, Vol. B, pp. 439–444, July 1999.

[11] P. S. Hingwe, *Robustness and Performance Issues in the Lateral Control of Vehicles in Automated Highway Systems*, Ph.D. Thesis, Univ. of California at Berkeley, 1997.

[12] S. Suryanarayanan and M. Tomizuka, "Observer based 'Look-ahead' scheme for fault tolerant lateral control of automated vehicles," *Proc. of the 5th Int. Symp. on Advanced Vehicle Control*, Ann Arbor, MI, pp. 269–274, Aug. 2000.

[13] P. Gahinet, A. Nemirovskii, A. J. Laub, and M. Chilali, "The LMI Control Toolbox," *Proc. of the 33rd CDC*, Lake Buena Vista, FL, pp. 2038–2041, 1994.

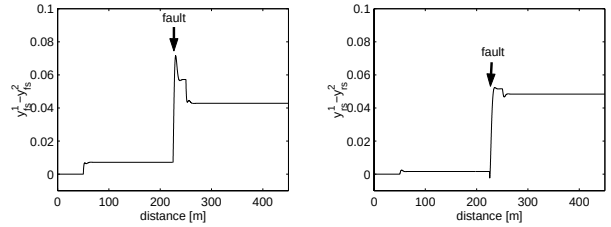

Figure 9: The estimation gap profiles, $\hat{y}_{fs}^1 - \hat{y}_{fs}^2$ (left) and $\hat{y}_{rs}^1 - \hat{y}_{rs}^2$ (right), of the re-tuned observers, $\hat{P}_1^{new}(s)$ and $\hat{P}_2^{new}(s)$.

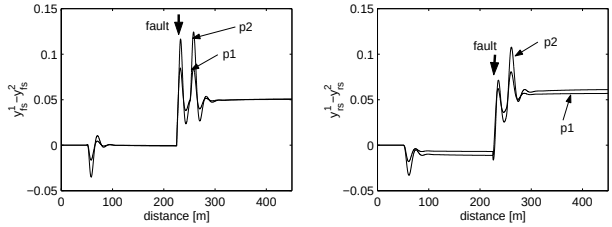

Figure 10: The estimation gap profiles, $\hat{y}_{fs}^1 - \hat{y}_{fs}^2$ (left) and $\hat{y}_{rs}^1 - \hat{y}_{rs}^2$ (right), of the re-tuned observers, $\hat{P}_1^{new}(s)$ and $\hat{P}_2^{new}(s)$, in two perturbed conditions ("p1" and "p2")